Plasma Chemistry and Plasma Processing (2026) 46:66
https://doi.org/10.1007/s11090-026-10675-3

ORIGINAL PAPER

Liquid-Phase Composition Modulates Reactive Oxygen and Nitrogen Species Formation During Nonthermal Dielectric Barrier Discharge Plasma Treatment

Kyoung Lee[1] · Munkhtsatsral Ganzorig[1,3] · Chuhyun Cho[2] · Yun-Sik Jin[2]

Received: 1 February 2026 / Accepted: 30 April 2026 / Published online: 22 May 2026
© The Author(s) 2026

Abstract

The accumulation of nitrification products, specifically nitric acid (HNO_3) and nitrous acid (HNO_2), along with reactive oxygen species (ROS) such as H_2O_2, was investigated following cold atmospheric-pressure dielectric barrier discharge (DBD) plasma treatment of various liquid phases. Plasma generated by a planar DBD with a mesh electrode positioned above deionized water produced nitrification products without detectable accumulation of H_2O_2. In contrast, methanol and ethanol promoted H_2O_2 accumulation. Other organic solvents, including ethyl acetate, *t*-butanol, hexane, acetonitrile, dichloromethane and acetone, also yielded nitrification products, with most solvents exhibiting concurrent H_2O_2 formation, except acetonitrile. To further elucidate the role of liquid-phase composition, selected additives, including ROS quenchers, were introduced into aqueous systems to probe specific reaction pathways, and their effects on pH, oxidation–reduction potential, and nitrification were examined. Notably, hydroxyl radical scavengers showed negligible effects on nitrification in deionized water. In acidic aqueous solutions, L-glutathione (GSH) underwent S-nitrosylation to form GS-NO, whereas in 10% methanol-water mixtures, GSH was additionally converted into oxidized products, including GS-CH_2OH, GSO_3H, and GSSG. Phenol in deionized water was primarily converted into 4-nitrosophenol, 2-nitrophenol, and 4-nitrophenol, without detectable oxygenated products. Overall, these results indicate that liquid-phase composition modifies plasma–liquid chemistry and stable product distributions.

Keywords Dielectric barrier discharge (DBD) · Organic solvent · Reactive oxygen species (ROS) · Nitrification · L-Glutathione · Phenol

✉ Kyoung Lee
kyounglee@changwon.ac.kr

[1] Department of Bio Health Science, Glocal Advanced Institute of Science and Technology, Changwon National University, Changwon 51140, Republic of Korea

[2] Korea Electrotechnology Research Institute, Changwon 51543, Republic of Korea

[3] Present address: Department of Biotechnology and Nutrition, School of Food, Light Industry and Design, Mongolian University of Science and Technology (MUST), Ulaanbaatar, Mongolia

Introduction

Cold atmospheric-pressure dielectric barrier discharge (DBD) plasma has emerged as a versatile platform for plasma-assisted liquid processing, owing to its ability to generate reactive oxygen and nitrogen species (ROS and RNS) under ambient conditions with relatively low energy input. In indirect DBD configurations, where the discharge is spatially separated from the liquid surface, reactive species are produced primarily in the gas phase and subsequently transported to the liquid through diffusion and interfacial reactions. This approach minimizes charge injection and joule heating in the liquid, allowing a clearer decoupling of gas-phase plasma chemistry from liquid-phase reaction pathways [1–3]. As a result, indirect DBD systems are increasingly employed for applications such as plasma-assisted nitrogen fixation, water treatment, and the generation of plasma treated liquids, where control over solution chemistry is critical [4–9].

In air-fed DBD plasmas, electron-impact reactions involving O_2 and N_2 initiate a complex network of gas-phase processes that can operate in distinct chemical regimes. Under typical conditions, ozone (O_3) is often the dominant long-lived oxidant; however, increasing discharge power, reduced electric field strength, or elevated gas temperature can shift the plasma into a nitrogen oxide (NO_x)-dominated regime. This transition is commonly attributed to enhanced vibrational excitation of N_2, which suppresses O_3 formation and promotes NO generation, followed by oxidation to higher nitrogen oxides [10–12]. When water vapor is present, additional pathways involving OH, HO_2, and related radicals further modify plasma chemistry, promoting the formation of longer-lived aqueous products such as H_2O_2, HNO_2/NO_2^-, and HNO_3/NO_3^- upon interaction with the liquid phase [13–15].

Importantly, the composition of the liquid phase, together with the reactor configuration and discharge conditions, strongly influences the fate of plasma-generated species during indirect DBD treatment. While short-lived species such as NO, NO_2, and O_3 exhibit limited persistence in water due to rapid secondary reactions or low solubility, stable products including H_2O_2, HNO_2/NO_2^-, HNO_3/NO_3^- have been reported to form and accumulate, ultimately define the chemical functionality of plasma-treated liquids [3, 5]. Previous studies have shown that modifying the aqueous matrix—through buffering, ionic strength, or the addition of organic cosolvents—can shift the balance between oxidative and nitrifying pathways [16, 17]. For example, plasma treatment of ethanol–water mixtures promotes the formation of HONOO/$ONOO^-$ and organic peroxide species, in addition to H_2O_2 and inorganic nitrogen species, highlighting solvent-enabled rerouting of plasma–liquid chemistry [17]. In addition, plasma treated oil phases have been reported to yield ROS, including H_2O_2 and carboxylic acids [18]. Such plasma-treated solutions have been associated with enhanced bioactivity, including wound-healing and antimicrobial effects. Nevertheless, systematic studies that directly correlate solvent identity with changes in ROS versus nitrification product distributions under indirect DBD operating conditions remain limited. In addition, the effects of various additives that can influence the distribution of reactive products have not been thoroughly studied.

In this study, we investigate how liquid-phase composition, including both solvents and aqueous additives, modulate the formation of ROS and nitrification products during indirect DBD plasma treatment under ambient air conditions. By introducing selected organic solvents and additives into deionized water, we evaluate changes in the relative accumulation of H_2O_2, HNO_2/NO_2^-, and HNO_3/NO_3^- while maintaining constant discharge param-

eters. The results demonstrate that, under NOx-dominated plasma conditions, liquid-phase composition modulates the accumulation and transformation of plasma-generated species, thereby influencing their relative distributions between oxidative and nitrifying products, and enabling rational tuning of plasma–liquid chemistry in indirect DBD systems.

Materials and Methods

Plasma Generation Setup

As shown in Fig. 1, which presents the side (a) view and mesh configuration (b) of the DBD discharge setup, the system consisted of a planar high-voltage (HV) electrode, a dielectric barrier, and a grounded mesh electrode supported by an insulating spacer. The entire assembly was enclosed in a box and operated under ambient, static air at room temperature (Supplementary Fig. S1).

The discharge electrode comprised an aluminum disk (Al, 60 mm in diameter, 10 mm thick) and a stainless-steel mesh (wire diameter: 0.25 mm, pitch: 1.2 mm, open area: 63%). A quartz plate (100 × 100 mm, thickness: 1 mm) was used as the dielectric barrier. To ensure high-voltage insulation between the electrodes, a fiberglass board (1.5 mm thick) was inserted, maintaining a 1.5 mm gap between the dielectric plate and the mesh electrode. The central part of the insulating spacer (discharge region) contained a circular opening with a diameter of 70 mm—slightly larger than that of the high-voltage electrode—allowing discharge between the electrodes. This configuration confined the plasma within the 70 mm region, minimized edge effects, and ensured uniform discharge over the electrode surface.

An aluminum cooling fin attached to the high-voltage electrode was externally cooled by forced airflow generated by a fan, enhancing heat dissipation and maintaining thermal stability during discharge operation. A Petri dish (70 mm in diameter, 15 mm in height) containing the treatment solution was placed in close contact beneath the mesh electrode. Chemically reactive species such as ROS and RNS generated by the DBD plasma were allowed to diffuse onto the liquid surface. In this experiment, 25 mL of solution was used, resulting in an approximately 5 mm gap was formed between the liquid surface and the mesh electrode. Although this gap was not completely open to the surrounding atmosphere, it was not sealed, allowing limited air exchange during plasma treatment. Thus, while bulk airflow into the gap was restricted, partial renewal of air could occur via diffusion and minor convective flow. During the 10 min plasma treatment, solvent loss was minimal and did not exceed 0.5 mL.

The input power consumption of the DBD plasma system was measured in real time using a commercially available power meter (SJPM-C16; Seojun Electric, Seoul, Korea; 220 V, 60 Hz; measurement range: 0.1–3520 W). The effective power dissipated in the DBD discharge was obtained by subtracting a constant baseline power of 14.8 W, corresponding to auxiliary devices (fan, lamps, etc.), from the total recorded power.

Chemicals and Standard Solutions

All chemicals and solvents used in this study were obtained from Sigma-Aldrich (Seoul, Korea), and were of the highest purity available. Ultrapure water (> 18 MΩ·cm) was pre-

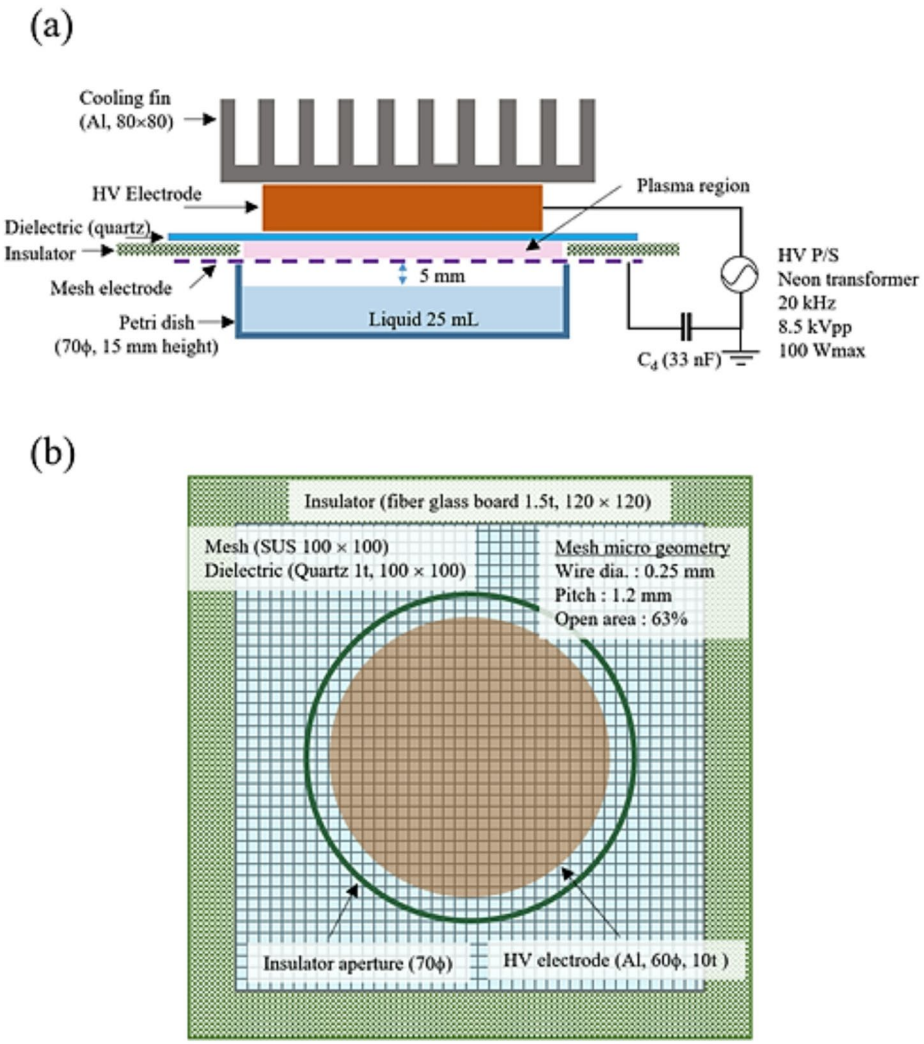

Fig. 1 Experimental schematics: (**a**) side view of the DBD discharge setup; (**b**) mesh configuration of the DBD discharge setup

pared using the Milli-Q system (Millipore, USA). Horseradish peroxidase (HRP, type II, salt-free) was obtained from Sigma-Aldrich (product number P8250-5KU).

Measurements of UV-Vis Absorbance Spectra, pH and ORP

The UV and Vis light absorption spectra were recorded using a nano-MD model spectrophotometer (Sinco Co., Korea). pH values were measured with a LAQUAtwin pH meter (Horiba, Japan). ORP was measured at room temperature using LAQUAact PC110 Ph/ORP/Cond Meter Set, 2ch Portable (Horiba, Japan). The instrument was calibrated prior to use with standards supplied by the vendor.

Quantification of HNO_2, HNO_3 and HCO_2H (Formic Acid) by Ion Chromatography (IC)

Immediately following plasma treatment, samples were diluted five-fold in 5 mM NaOH solution. Products formed in water-insoluble solvents such as hexane and dichloromethane were extracted using four volumes of NaOH solution, resulting in near-complete extraction. The concentrations of HNO_2, HNO_3 and formic acid were determined using IC (881 Compact IC pro 1, Metrohm AG, Switzerland) equipped with a Metrosep A Supp 5 column (4 × 150 mm). The column was eluted with a mobile phase consisting of 3.2 mM Na_2CO_3 and 1.0 mM $NaHCO_3$ at a flow rate of 0.7 mL/min at 30 °C. Under these conditions, HCO_2^-, NO_2^- and NO_3^- were detected at retention times of 4.69 min, 6.60 min, and 9.20 min, respectively. Quantification was performed using calibration curves generated from standard solutions.

Quantification of H_2O_2

Hydrogen peroxide was measured using the phenol red–HRP method [19] with minor modifications. Reactions were conducted in modified PBS (10 mM potassium phosphate, 140 mM NaCl, pH 7.0). Phenol red (0.56 mM) and HRP (2 mg/mL stock) were freshly prepared in modified PBS. A 1 mM H_2O_2 stock was prepared from 30% H_2O_2 immediately before use and verified at 230 nm (ε = 81 /M·cm) [19]. For each assay, phenol red solution (900 µL) and HRP (20 µL; final 40 µg or 8.8 U/mL) were mixed, followed by addition of 20–40 µL of sample or standard to a final volume of 1.0 mL Plasma-treated samples were diluted tenfold with deionized water, except for deionized water, 5% methanol, acetonitrile, and dichloromethane samples, which were analyzed without dilution. For water-immiscible solvents, extraction recovery yields determined using H_2O_2 standards were applied. After incubation at 37 °C for 30 min, reactions were terminated with 10 µL of 1 N NaOH, and absorbance was measured at 610 nm. Controls for each reaction were also conducted without HRP. H_2O_2 concentrations were determined from a calibration curve (0–60 µM). The detection limit, calculated with respect to the original solutions, was approximately 50 µM.

Kinetic Measurement of S-nitrosylation of GSH in PAW

For this experiment, a solution containing 10 mM GSH in deionized water was employed. Throughout the plasma treatment, 0.1 mL aliquots were withdrawn and subsequently diluted tenfold using deionized water. Absorbance measurements were conducted by scanning the wavelength range from 200 to 900 nm. The product, *S*-nitrosoglutathione (GS-NO) was assessed using an extinction coefficient of 922 / M·cm at a maximum wavelength (λ_{max}) of 335 nm [20].

Mass Spectrometry

Mass analysis of GSH and its derivatives was performed using a Q Exactive Plus Quadrupole-Orbitrap Mass Spectrometer controlled by Xcalibur software (Thermo Scientific, USA). Samples, diluted in deionized water, were directly infused into the system at a flow rate of 10 µl/min. The electrospray ionization spray voltage was set at 3.50 kV for negative ion mode and 2.50 kV for positive ion mode. The ion transfer capillary temperature was

maintained at 320 °C. Gas settings included a sheath gas N_2 pressure of 15 arbitrary units, the auxiliary gas pressure to 5 arbitrary units, and the sweep gas pressure to 0 atm. The auxiliary gas temperature was kept at 100 °C. Mass spectra were recorded in the *m/z* range of 100–700. For MS/MS, stepped normalized collision energy of 10 and 20 were applied.

Gas-Chromatography-Mass Spectrometry (GC-MS) Analysis

A solution containing 10 mM phenol in deionized water, with or without additives, was subjected to plasma treatment for 10 min. Following the reaction, 10 mL of each solution was transferred to 15-mL Falcon tubes, and 2 mL ethyl acetate was added and vortexed. After centrifugation at 13,000 rpm for 5 min, the upper ethyl acetate layers were collected for GC-MS analysis. GC-MS analysis was performed using a capillary column (Perkin Elmer Elite-5ms, 0.25 mm × 30 m, 0.25 μm film thickness) with modifications to a previously described method [21]. The column temperature was initially held at 40 °C for 5 min, then ramped from 40 to 300 °C at a rate of 10 °C/min. Helium gas used as a carrier gas at a flow rate of 1 mL/min. Products were identified by comparing them to standard substances, and the relative quantities were determined by integrating the respective peak areas.

Results and Discussion

Power Consumption During DBD Plasma Discharge

The chemistry of cold atmospheric-pressure DBD plasma treatment at the surface of deionized water and organic solvents was investigated using a Petri dish–based liquid-phase reactor, in which plasma was generated above a mesh electrode without direct contact with the liquid (Fig. 1). Lissajous-based power dissipation is commonly used in DBD experiments because it directly reflects the energy dissipated within the discharge, independent of external circuit losses. However, under solvent-dependent discharge conditions, stable Q–V loops could not be reproducibly obtained. Therefore, power consumption measured at the power supply level was used instead. Although this metric does not directly represent the power dissipated at the plasma–liquid interface, it provides a robust and reproducible basis for comparing solvent-dependent electrical behavior under identical operating conditions.

Figure 2 presents the time-dependent power consumption during DBD plasma discharge for different liquid phases. Although no abrupt solvent-specific differences were observed, the results can be broadly classified into two groups. Atmospheric air, deionized water, methanol, ethanol, ethyl acetate, and acetone exhibited nearly constant power consumption throughout the 10 min treatment period. In contrast, acetonitrile, hexane, *t*-butanol, and dichloromethane showed a gradual decrease in power consumption, with the effect most pronounced for dichloromethane. For the solvents in this latter group, the observed trend is consistent with increased solvent vapor in the interelectrode region, which can affect electron transport and enhance energy-loss collisions, thereby reducing discharge intensity [3]. However, this behavior cannot be explained by vapor pressure alone; for example, although acetone has a higher vapor pressure than *t*-butanol, they exhibit opposite trends, indicating that electron energy dissipation, quenching, and solvent-specific reaction pathways also play important roles [3, 22]. For most solvents, the liquid temperature increased to approx-

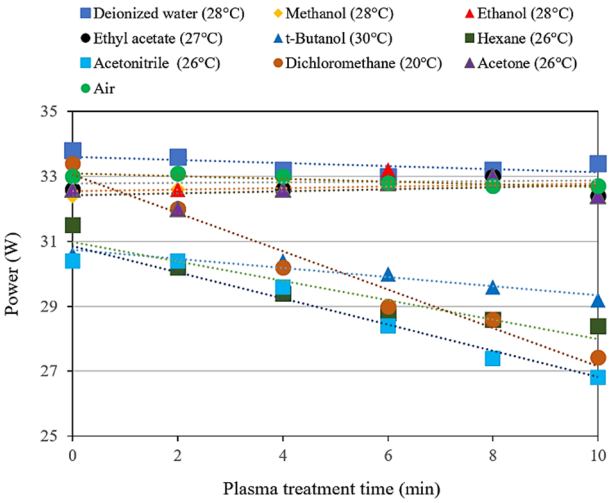

Fig. 2 Time-dependent power consumption of the DBD plasma during treatment. Data represent the mean of three measurements; SD (< 5%) is omitted for clarity. Temperatures shown in parentheses for each solvent correspond to values measured after 10 min of plasma treatment; the initial temperature was 19 °C

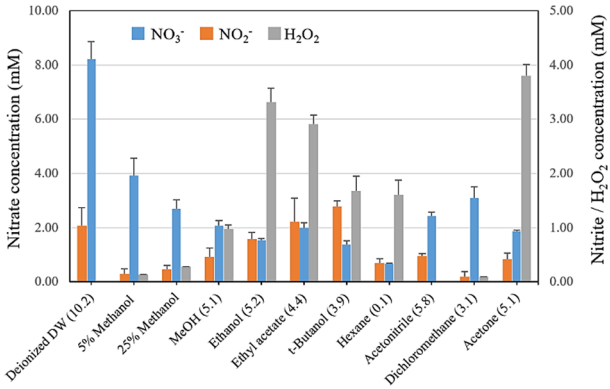

Fig. 3 Production of HNO_3, HNO_2, and H_2O_2 in the liquid phase after 10 min of plasma treatment. Numbers in parentheses following each solvent indicate the polarity index. Data are presented as the mean ± SD from three independent measurements

imately 26–30 °C after 10 min of plasma treatment, whereas no significant temperature change was observed for dichloromethane.

Influence of Solvent Composition on Plasma-Induced Nitrification and H_2O_2 Formation

The effects of these solvents on the concentrations of nitrification products and H_2O_2 are summarized in Fig. 3. For deionized water, the concentrations of nitrification products after 10 min of plasma treatment reached 8.2 ± 0.6 mM for HNO_3 and 1.0 ± 0.3 mM for HNO_2. In contrast, H_2O_2 was not detected in deionized water, with a detection limit of 50 µM. When methanol was added to water at concentrations of 5% and 25% (v/v), nitrate formation decreased to approximately 47.4% and 32.7% of the value observed in deionized water, respectively, while measurable accumulation of H_2O_2 was observed (Fig. 3).

Plasma treatment was further examined using solvents spanning a wide range of polarity and water miscibility, including polar, water-miscible solvents (ethanol, *t*-butanol, acetone, and acetonitrile), moderately polar but sparingly soluble solvents (ethyl acetate and dichlo-

romethane), and a nonpolar, water-immiscible solvent (hexane), with their corresponding polarity indices [23] shown in Fig. 3. In methanol-containing systems, nitrate formation decreased to approximately 24.3% of that observed in deionized water, whereas H_2O_2 accumulated to concentrations of approximately 1 mM. In addition, plasma treatment of methanol resulted in the accumulation of formate, reaching 14.8 mM after 10 min, indicating extensive oxidation reactions, whereas formate was not detected in plasma-treated water (Supplementary Fig. S2).

Across all solvent systems examined, nitrate accumulation was observed, whereas H_2O_2 accumulation was solvent dependent. H_2O_2 was not detected in deionized water or acetonitrile and was present only at trace levels in dichloromethane, while measurable accumulation was observed in the remaining solvents (Fig. 3). No clear linear dependence of H_2O_2 concentration on solvent polarity was observed. In solvents lacking water, H_2O_2 formation may proceed via solvent-derived radical pathways, as exemplified by methanol. In methanol-containing systems, electron impact dissociation of the solvent cleaves the weak C–H bond, generating $CH_2OH\cdot$ and H radicals, which subsequently react with O_2 either directly via $H + O_2 \rightarrow HO_2$ or indirectly through $CH_2OH\cdot$-derived peroxyl intermediates that decompose to formaldehyde and additional HO_2 radicals, which may subsequently recombine to form H_2O_2 ($2HO_2 \rightarrow H_2O_2 + O_2$) [24, 25]. Detailed mechanistic studies on the formation pathways of nitrate and H_2O_2 in organic solvents remain to be conducted.

Under our experimental conditions, the yields of nitrification products such as NO_3^- and NO_2^- exhibited a weak but reproducible positive correlation ($R^2 \approx 0.70$) with the solvent polarity index (Supplementary Fig. S3). Highly polar solvents such as H_2O ($P = 10.2$) produced the highest nitrification product concentration (8.8 mM), whereas nonpolar hexane ($P = 0.1$) yielded only 1.0 mM. This trend reflects enhanced stabilization of nitrogen oxides in polar, hydrogen-bonding media, indicating that high solvent polarity and protic character favor NO_x-dominated plasma–liquid interactions.

Effect of Additives on Nitrification Product Formation by Plasma Treatment of Deionized Water

Our initial findings indicated that organic solvents, or deionized water containing methanol, negatively affected HNO_3 production. To further elucidate the factors influencing nitrification product formation, additional experiments were conducted by introducing various additives to deionized water (Table 1). These included OH radical quenchers (mannitol, sodium formate) [26, 27]; OH radical and $^1O_2$ quenchers (L-histidine, phenol, L-ascorbic acid, DL-dithiothreitol, L-tryptophan) [13, 27–29]; OH radical, $^1O_2$ and NO quencher (GSH) [28, 30]; N_2O_3 (N^+) and OH quencher (NaN_3) [31, 32]; and other chemicals such as H_2O_2, $NaNO_2$, NaOH, HCl, and $FeSO_4\cdot 7H_2O$. Several of these, including L-ascorbic acid, DL-dithiothreitol and GSH, are strong reducing compounds. The solutions in the Petri dish were treated with plasma for 10 min, after which HNO_3 and HNO_2 were quantified by IC.

Most additives did not significantly affect HNO_3 production, which largely remained close to the control level of 8.5 mM. However, notable increases (> 10%) were observed with 20 mM solutions of H_2O_2 (111.5%), $NaNO_2$ (116.2%), and HCl (117.3%). In contrast, moderate decreases (< 10%) were observed with 10 mM phenol (90.5% of control), 10 mM L-ascorbic acid (90.5%) and 10 mM GSH (82.4%). HNO_2 was detected at approximately 1 mM in most solutions containing additives, except in solutions containing H_2O_2, HCl,

Table 1 Chemical properties of plasma water with added chemicals before and after plasma exposure[#]

Added chemical	Known function	NO_3^- (mM)	NO_2^- (mM)	pH		ORP (mV)	
				t=0 min	t=10 min	t=0 min	t=10 min
Control (H_2O)		8.5 ± 0.7	1.0 ± 0.1	5.4 ± 0.0	2.0 ± 0.0	70 ± 6	572 ± 7
D-Mannitol	OH quencher	8.7 ± 0.6	1.0 ± 0.0	5.3 ± 0.3	2.0 ± 0.0	82 ± 7	616 ± 2
Sodium formate	OH quencher	8.6 ± 1.1	1.0 ± 0.1	6.4 ± 0.1	3.6 ± 0.0	101 ± 3	470 ± 2
L-Histidine	$^1O_2$ and OH quenchers	8.6 ± 0.2	0.9 ± 0.0	4.0 ± 0.0	2.2 ± 0.0	160 ± 2	603 ± 1
Phenol	$^1O_2$ and OH quenchers	7.7 ± 0.6	0.8 ± 0.0	4.6 ± 0.1	2.0 ± 0.0	107 ± 2	594 ± 0
L-Ascorbic acid	$^1O_2$ and OH quenchers	7.7 ± 0.9	0.0± 0.0	3.0 ± 0.0	2.1 ± 0.0	146 ± 3	152 ± 0
L-Glutathione	$^1O_2$, OH and NO quenchers	7.09 ± 0.9	1.5 ± 0.2	3.3 ± 0.0	2.5 ± 0.1	80 ± 6	154 ± 2
DL-Dithiothreitol	$^1O_2$ and OH quenchers	8.8 ± 0.7	1.1 ± 0.0	5.6 ± 0.2	2.5 ± 0.0	-181 ± 6	19 ± 4
L-Tryptophan	$^1O_2$ and OH quenchers	8.9 ± 0.6	0.5 ± 0.0	6.7 ± 0.1	2.6 ± 0.0	38 ± 5	532 ± 6
H_2O_2	Presumed NO_3^- precursor	9.5 ± 0.5	0.0 ± 0.0	4.4 ± 0.1	2.0 ± 0.0	275 ± 2	560 ± 9
$NaNO_2$	Presumed NO_3^- precursor	9.9 ± 0.7	10.8 ± 0.2	6.2 ± 0.1	3.2 ± 0.0	240 ± 7	526 ± 6
NaOH	pH increase	8.8 ± 1.0	1.2 ± 0.1	11.8 ± 0.0	11.0 ± 0.1	-96 ± 8	-29 ± 9
HCl	pH decrease	10.0 ± 0.4	0.0 ± 0.0	1.8 ± 0.0	1.5 ± 0.0	403 ± 9	641 ± 1
$FeSO_4 \cdot 7H_2O$	Reducing agent	8.1 ± 0.7	0.9 ± 0.0	3.4 ± 0.0	2.4 ± 0.0	266 ± 5	423 ± 3
NaN_3	N_2O_3 (N^+), OH quenchers	-	1.1 ± 0.1	6.8 ± 0.0	4.9 ± 0.0	89 ± 0	140 ± 11

All chemicals were at 20 mM, except L-glutathione (10 mM), DL-dithiothreitol (10 mM), L-tryptophan (5 mM). Solutions were exposed to plasma for 10 min. t=0 refers to the initial conditions with deionized water before treatment. Data are represented as mean ± SD from three independent experiments. ORP, oxidation-reduction potential.

- Not measurable

and L-ascorbic acid, where it was not detected (Table 1). In these specific solutions, the characteristic absorbance peaks of nitrous acid around 358 nm [33, 34] were also absent in spectrophotometric analysis.

Previous studies have reported that prolonged exposure of water to air-fed cold DBD plasma under ambient conditions is associated with solution acidification and elevated oxidation–reduction potential (ORP) [35, 36]. The observed pH decrease is mainly attributed to the formation of strong acids, HNO_3 and HNO_2. In the present study, most solutions containing the tested additives reached final pH values in the range of 2.0–2.5, comparable to those of deionized water (Table 1). However, some variations were observed with solutions containing HCl, NaOH, sodium formate, $NaNO_2$, and NaN_3. Specifically, the addition of sodium formate resulted in a final pH value of 3.6 ± 0.0, while $NaNO_2$ led to a pH of 3.2 ± 0.0. These values are consistent with their buffering capacities, considering the pKa values of 3.75 for HCOOH (formic acid) [37] and 3.16 for HNO_2 [38]. Furthermore, the presence of 20 mM NaN_3 led to a final pH of 4.9 ± 0.0 (pKa of HN_3 = 4.65) [39]. In this specific case, quantification of NO_3^- by IC was not possible because the N_3^- and NO_3^- peaks coeluted. Nevertheless, the observed pH drop indicated the production of nitric acid.

Effects of Plasma Treatment on ORP of Deionized Water with Additives

The ORP quantifies the oxidation state of a solution, with higher values reflecting a stronger oxidative environment. ORP changes were measured in solutions containing additives following plasma exposure (Table 1). In deionized water, ORP increased from 70 ± 6 mV to 572 ± 7 mV after a 10-min plasma treatment, consistent with the accumulation of oxidizing agents. Although low ORP values are generally associated with high pH levels [34], solutions containing L-ascorbic acid, DL-dithiothreitol, $FeSO_4 \cdot 7H_2O$, and GSH exhibited smaller ORP increases, indicating partial scavenging of plasma-generated oxidizing species through their own oxidation. Specifically, L-ascorbic acid exhibited a decrease in absorbance at 264 nm, indicating its oxidation (Supplementary Fig. S4a) [40]. Similarly, DL-dithiothreitol and $FeSO_4 \cdot 7H_2O$ exhibited absorption spectra characteristic of oxidation after

plasma exposure [41] (Supplementary Fig. S4b and Fig. S5). Changes in visible absorbance spectra and GSH oxidation are described in the following section.

Stimulation of GSH S-Nitrosylation at Low pH and Its Inhibition by Alcoholic Solvents and NaN_3

GSH was used as a reaction probe to examine potential differences in the chemistry of plasma-treated water in the presence of additives. The sulfur element in GSH is recognized as the primary site for S-nitrosylation by NO_x generated both in vitro and in vivo [42]. Because GS-NO has a high molar extinction coefficient, the extent of *S*-nitrosylation during the plasma treatment could be sensitively detected. When 10 mM GSH in deionized water was treated, RS-NO formation proceeded almost linearly after an initial lag of about 2 min, showing a rate of 0.34 mM/min during the subsequent 8 min (Fig. 4a). After 10 min of plasma treatment, approximately 3.0 mM of RS-NO was produced.

To further elucidate the S-nitrosylation mechanism, reaction-probing additives were introduced during plasma treatment of GSH in deionized water. Figure 4b presents the relative rates of product formation during the 2–8 min interval of plasma treatment. In the presence of 20 mM mannitol or 20 mM L-histidine, known OH scavengers, the rates were 93.3%, and 94.8%, respectively, relative to deionized water. In contrast, 1.0% methanol reduced the rate to 26.3%. The addition of 20 mM ascorbic acid also lowered the rate to 71.0%.

The GS-NO formation rate was reduced to 20.0% in the presence of 20 mM NaN_3 (Fig. 4b). Given that the final pH after plasma treatment was 4.4 and the pKa of HN_3 is 4.65, we investigated whether the pH change contributed to this diminished rate. To examine this, 20

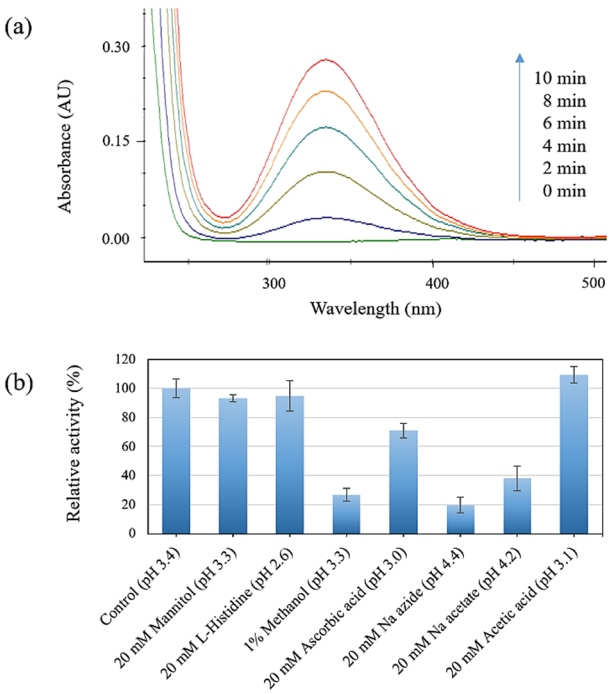

Fig. 4 Spectroscopic analysis of GS-NO formation during plasma treatment of 10 mM GSH. (**a**) Absorbance spectra at the indicated incubation times in deionized water, recorded after 10-fold dilution. (**b**) Relative GS-NO formation rate in deionized water with various additives. pH values are indicated after treatment. Data are represented as mean ± SD from three independent measurements

mM sodium acetate (pKa = 4.75) was used as a buffer with a comparable pKa. Under these conditions, the rate of GS-NO formation was 37.9% of the control, with a resultant pH of 4.2 (Fig. 4b). By contrast, 20 mM acetic acid alone fully restored the formation rate to the level observed with deionized water. These findings indicate that the reduced rate of GS-NO formation in the presence of NaN_3 arises from both its buffering effect and its intrinsic inhibitory activity, as NaN_3 is known to scavenge OH [31] and N_2O_3 [32].

The potential roles of HNO_2 and HNO_3 in mediating GS–NO formation from GSH under plasma-free conditions were examined. When deionized water containing 2.0 mM $NaNO_2$ and 10 mM GSH in 20 mM HCl was incubated for 1 h at room temperature, 1.6 ± 0.1 mM GS-NO formed. This result indicates that HNO_2 can S-nitrosylate GSH under acidic conditions, consistent with previous reports showing that GSNO is efficiently formed by the reaction of GSH with nitrous acid [43]. This pathway relies on strong electrophilic nitrosating agents such as N_2O_3 and the nitrosonium ion (NO^+), which directly react with GSH to form GS-NO [44, 45]. In contrast, no GS-NO formation was observed with HNO_3 under the same incubation conditions.

GSH products formed by plasma discharge in the liquid phase were identified using mass spectrometry, as described in the 'Materials and Methods'. In deionized water, the ESI spectrum in positive mode (Fig. 5a) showed a signal at m/z = 337.08, corresponding to the proton adduct of GS-NO ($[GS\text{-}NO+H]^+$), along with the proton adduct of the substrate GSH (m/z = 308.09, $[GSH+H]^+$). In negative mode, the corresponding deprotonated molecules were detected at *m/z* = 335.07 ($[GS\text{-}NO\text{-}H]^-$) and 306.07 ($[GSH\text{-}H]^-$), respectively (Fig. 5b). In addition, the nitrate adducts of GSH ($[GSH+NO_3]^-$) and GS-NO ($[GS\text{-}NO+NO_3]^-$) were also detected at m/z = 369.07 and 398.06, respectively (Fig. 5b).

In contrast, in the presence of 10% methanol, a major product with *m/z* = 338.01 was detected in positive mode (Fig. 5c). This product exhibited a dominant fragment at 308.0 Da ($[GSH+H]^+$) in MS/MS analysis (Supplementary Fig. S6a), and was identified as S-hydroxymethyl glutathione ($GS\text{-}CH_2OH$). The protonated forms of glutathione sulfonic acid (GSO_3H, m/z = 356.07, $[GSO_3H+H]^+$) and glutathione disulfide (GS-SG, m/z = 613.16, $[GS\text{-}SG+H]^+$), both oxidized derivatives of GSH, were also detected. In negative mode, the corresponding deprotonated forms of GSO_3H (m/z = 354.06, $[GSO_3]^-$) and GS-SG

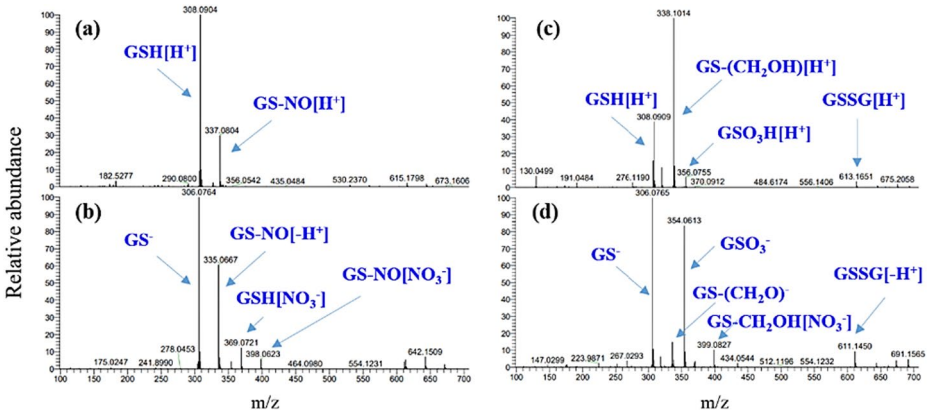

Fig. 5 Mass analysis of GSH solutions after 10 min of plasma treatment. (**a**, **c**) ESI positive mode for deionized water and 10% methanol in deionized water, respectively. (**b**, **d**) ESI negative mode for deionized water and 10% methanol in deionized water, respectively. Adducts are indicated in brackets

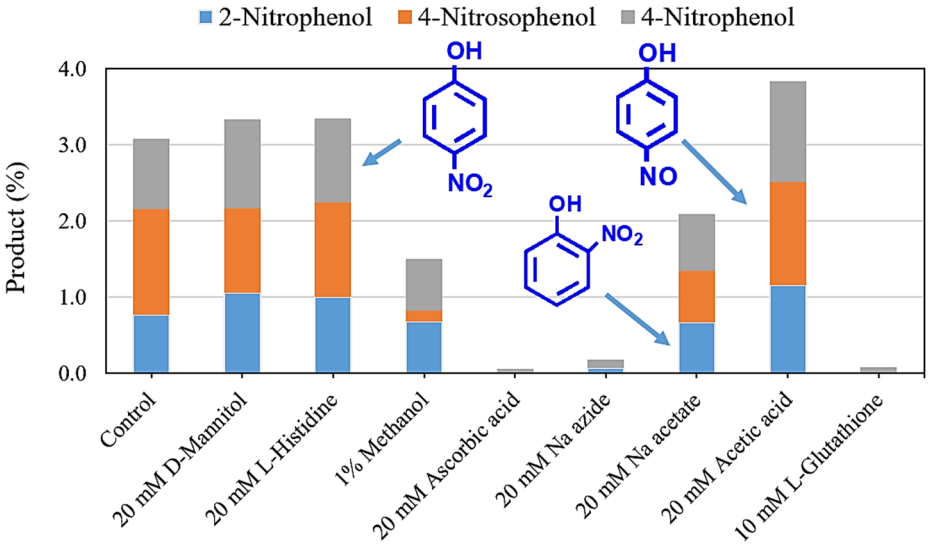

Fig. 6 Product distribution formed from 10 mM phenol solutions after 10 min of plasma treatment. Additives are indicated. Data represent the mean of three measurements; SD (<5%) is omitted for clarity

(m/z=611.14, [GS-SG-H$^-$]) were observed. Additionally, a peak at m/z=399.08, with a major fragment at 306.0 Da and a minor fragment at 336.05 Da in MS/MS analysis (Fig. S6b), was identified as the nitrate adduct of GS-CH_2OH ([GS-CH_2OH+NO_3]$^-$) (Fig. 5d).

In brief, plasma exposure in deionized water led to efficient S-nitrosylation of GSH under acidic conditions, whereas the presence of methanol or the addition of NaN_3 markedly suppressed GS-NO formation. In contrast, GS-NO formation was not significantly affected by hydroxyl radical scavengers. Methanol-containing systems instead promoted oxidative modification of GSH, yielding various oxidized GSH products in addition to GS-NO and indicating a solvent-dependent shift in dominant reaction pathways. Together, these results confirm distinct differences between nitrative and oxidative reaction pathways in deionized water with or without methanol during DBD treatment as shown in Fig. 3.

Analysis of Products Formed from Phenol by Plasma Treatment

To further investigate the reaction mechanisms of plasma-treated water, phenol was employed as a reaction probe. GC-MS analysis revealed that plasma treatment of 10 mM phenol for 10 min converted approximately 0.3 mM of the substrate into products, with 2-nitrosophenol, 2-nitrophenol, and 4-nitrophenol produced in nearly equimolar amounts (Fig. 6). Under these conditions, nitrate and nitrite reached 90% and 83%, respectively, of those measured in plasma-treated deionized water (Table 1). The effects of additives closely mirrored those observed for GSH S-nitrosylation (Fig. 5b): D-mannitol and L-histidine had no significant effect, whereas methanol, ascorbic acid, NaN_3, and acetate inhibited product formation. The addition of 10 mM GSH also almost completely suppressed phenol conversion. Notably, ascorbic acid and NaN_3 nearly abolished product formation, in contrast to their more moderate inhibitory effects on GSH S-nitrosylation. Although detected only in trace amounts, 4-nitrophenol was the common product formed in the presence of these

substrates and GSH. Furthermore, inhibition by acetate was reversed by acetic acid, which yielded even higher product levels than the control. This suggests that, similar to GSH S-nitrosylation, phenol nitration is promoted under acidic conditions. Notably, oxygenation products such as catechol and hydroquinone were not detected. This contrasts with previous studies involving direct plasma–liquid contact, where significant H_2O_2 accumulation promoted hydroxylation pathways [46]. The absence of net H_2O_2 accumulation in our system likely shifts the chemistry toward electrophilic substitution reactions under acidic conditions, favoring nitrosophenol and nitrophenol formation [47].

Although organic solvents are not intended for direct application, they were used here as model systems to systematically examine how liquid-phase properties affect plasma–liquid interactions. In practical systems, comparable effects can arise from dissolved organic matter, inorganic ions, or biomolecules, which influence the formation, transformation, and persistence of ROS and RNS. In plasma-based water treatment and advanced oxidation processes, the composition of the liquid phase has been shown to affect the balance between short-lived radicals and longer-lived oxidants, thereby influencing treatment efficiency and selectivity [3, 46, 48] Similarly, in biomedical plasma applications, the surrounding chemical environment plays a critical role in determining the types and concentrations of ROS and RNS delivered to biological targets, ultimately affecting cellular responses and therapeutic outcomes [49]. Therefore, the present results contribute to a mechanistic understanding of how liquid-phase composition can be used to regulate reactive species distributions in plasma–liquid systems.

Conclusion

This study demonstrates that liquid-phase composition strongly influences reactive species formation during the indirect treatment of liquids with nonthermal DBD plasma. In deionized water, acidic conditions combined with limited ROS accumulation are associated with a predominance of nitrification and electrophilic nitrosation pathways, whereas organic solvents are associated with increased accumulation of oxidative products, including peroxide formation. These results can be attributed to solvent-dependent modulation of plasma–liquid interfacial chemistry, while the primary reaction regime remains governed by the plasma (e.g., NOx-dominated conditions), potentially involving differences in the formation levels of key NO_x intermediates and changes in reaction environments at the gas–liquid interface. Furthermore, the additives employed in this study provide useful probes for influencing interfacial reaction pathways and for elucidating underlying reaction mechanisms.

Supplementary Information The online version contains supplementary material available at https://doi.org/10.1007/s11090-026-10675-3.

Acknowledgements This research received funding from the ‘Mid-career Faculty Research Support Grant’ at Changwon national University in 2025. This study was conducted using equipment at the CWNU Gyeongnam Bio and Anti-Aging Core Facility Center.
This research was also supported by Korea Electrotechnology Research Institute (KERI) Primaryresearch program through the National Research Council of Science and Technology (NST) funded bythe Ministry of Science and ICT (MSIT) under Grant 26A01044.

Author Contributions K.L. conceptualized and supervised the study, participated in the investigation, performed experiments and data analysis, prepared the manuscript, and acquired funding; M.G. performed

experiments and data analysis; C.C. designed and fabricated the instrumentation, performed experiments and data analysis, and edited the manuscript; Y-S.J. administered the project, contributed to instrument design and fabrication, acquired funding, and edited the manuscript.

Funding This work was supported by the Korea Electrotechnology Research Institute (KERI) Primary Research Program through the National Research Council of Science and Technology (NST) funded by the Ministry of Science and ICT (MSIT) (Grant No. 19A01011 and Grant 26A01044) and by the National Research Foundation of Korea (NRF), funded by MSIT (Grant No. RS-2025-23523128).

Data Availability Data will be made available on request.

Declarations

Competing interests The authors declare no competing interests.

Open Access This article is licensed under a Creative Commons Attribution-NonCommercial-NoDerivatives 4.0 International License, which permits any non-commercial use, sharing, distribution and reproduction in any medium or format, as long as you give appropriate credit to the original author(s) and the source, provide a link to the Creative Commons licence, and indicate if you modified the licensed material. You do not have permission under this licence to share adapted material derived from this article or parts of it. The images or other third party material in this article are included in the article's Creative Commons licence, unless indicated otherwise in a credit line to the material. If material is not included in the article's Creative Commons licence and your intended use is not permitted by statutory regulation or exceeds the permitted use, you will need to obtain permission directly from the copyright holder. To view a copy of this licence, visit http://creativecommons.org/licenses/by-nc-nd/4.0/.

References

1. Kogelschatz U (2003) Dielectric-barrier discharges: their history, discharge physics, and industrial applications. Plasma Chem Plasma Process 23:1–46. https://link.springer.com/article/10.1023/A:1022470901385
2. Graves DB (2012) The emerging role of reactive oxygen and nitrogen species in redox biology and some implications for plasma applications to medicine and biology. J Phys D:Appl Phys 45:263001. https://doi.org/10.1088/0022-3727/45/26/263001
3. Bruggeman PJ, Kushner MJ, Locke BR, Gardeniers JG, Graham W, Graves DB, Hofman-Caris R, Maric D, Reid JP, Ceriani E (2016) Plasma–liquid interactions: a review and roadmap. Plasma Sources Sci Technol 25:053002. https://doi.org/10.1088/0963-0252/25/5/053002
4. Jin YS, Cho C (2019) Generation of plasma activated water by a hybrid plasma source. IEEE Trans Plasma Sci 47:4588–4592. https://doi.org/10.1109/TPS.2019.2944171
5. Jablonowski H, Santos Sousa J, Weltmann K-D, Wende K, Reuter S (2018) Quantification of the ozone and singlet delta oxygen produced in gas and liquid phases by a non-thermal atmospheric plasma with relevance for medical treatment. Sci Rep 8:12195. https://doi.org/10.1038/s41598-018-30597-4
6. Kong MG, Kroesen G, Morfill G, Nosenko T, Shimizu T, Van Dijk J, Zimmermann J (2009) Plasma medicine: an introductory review. New J Phys 11:115012. https://doi.org/10.1088/1367-2630/11/11/115012
7. Mouele ESM, Tijani JO, Badmus KO, Pereao O, Babajide O, Fatoba OO, Zhang C, Shao T, Sosnin E, Tarasenko V (2021) A critical review on ozone and co-species, generation and reaction mechanisms in plasma induced by dielectric barrier discharge technologies for wastewater remediation. J Environ Chem Eng 9:105758. https://doi.org/10.1016/j.jece.2021.105758
8. Jin YS, Cho C, Kim D, Sohn CH, Ha C-s, Han S-T (2020) Mass production of plasma activated water by an atmospheric pressure plasma. Jpn J Appl Phys 59:SHHF05. https://doi.org/10.35848/1347-4065/ab8c84
9. Zhou R, Zhou R, Wang P, Xian Y, Mai-Prochnow A, Lu X, Cullen P, Ostrikov KK, Bazaka K (2020) Plasma-activated water: Generation, origin of reactive species and biological applications. J Phys D:Appl Phys 53:303001. https://doi.org/10.1088/1361-6463/ab81cf

10. Shimizu T, Sakiyama Y, Graves DB, Zimmermann JL, Morfill GE (2012) The dynamics of ozone generation and mode transition in air surface micro-discharge plasma at atmospheric pressure. New J Phys 14:103028. https://doi.org/10.1088/1367-2630/14/10/103028
11. Park S, Choe W, Jo C (2018) Interplay among ozone and nitrogen oxides in air plasmas: Rapid change in plasma chemistry. Chem Eng J 352:1014–1021. https://doi.org/10.1016/j.cej.2018.07.141
12. Xi W, Luo S, Liu D, Wang Z, Liu Z, Guo L, Wang X, Rong M (2022) The effect of humidity on the discharge mode transition of air discharge plasma. Phys Plasmas. https://doi.org/10.1063/5.0107803
13. Lukes P, Clupek M, Babicky V, Janda V, Sunka P (2005) Generation of ozone by pulsed corona discharge over water surface in hybrid gas–liquid electrical discharge reactor. J Phys D:Appl Phys 38:409. https://doi.org/10.1088/0022-3727/38/22/005
14. Tian W, Kushner MJ (2014) Atmospheric pressure dielectric barrier discharges interacting with liquid covered tissue. J Phys D:Appl Phys 47:165201. https://doi.org/10.1088/0022-3727/47/16/165201
15. Liu D, Liu Z, Chen C, Yang A, Li D, Rong M, Chen H, Kong M (2016) Aqueous reactive species induced by a surface air discharge: Heterogeneous mass transfer and liquid chemistry pathways. Sci Rep 6:23737. https://doi.org/10.1038/srep23737
16. Bae JH, Huh S-C, Rahdar N, Park S (2026) Real-time formation of nitrate and nitrite species in plasma-activated liquids: from distilled water to cell culture solutions. Plasma Chem Plasma Process 46:21. https://doi.org/10.1007/s11090-026-10638-8
17. Li Y, Liu J, Zhao F, Song K, Nie L, Liu D, Lu X (2023) Plasma-activated ethanol solution and it's decontamination effect. High Voltage 8:833–840. https://doi.org/10.1049/hve2.12299
18. Zou X, Xu M, Pan S, Gan L, Zhang S, Chen H, Liu D, Lu X, Ostrikov KK (2019) Plasma activated oil: Fast production, reactivity, stability, and wound healing application. ACS Biomater Sci Eng 5:1611–1622. https://doi.org/10.1021/acsbiomaterials.8b01335
19. Pick E, Keisari Y (1980) A simple colorimetric method for the measurement of hydrogen peroxide produced by cells in culture. J Immunol Methods 38:161–170. https://doi.org/10.1016/0022-1759(80)90340-3
20. Hart TW (1985) Some observations concerning the S-nitroso and S-phenylsulphonyl derivatives of L-cysteine and glutathione. Tetrahedron Lett 26:2013–2016. https://doi.org/10.1016/S0040-4039(00)98517-3
21. Cho MC, Kang D-O, Yoon BD, Lee K (2000) Toluene degradation pathway from *Pseudomonas putida* F1: substrate specificity and gene induction by 1-substituted benzenes. J Ind Microbiol Biotechnol 25:163–170. https://doi.org/10.1038/sj.jim.7000048
22. Dahiru UH, Saleem F, Zhang K, Harvey A (2022) Plasma-assisted removal of methanol in N_2, dry and humidified air using a dielectric barrier discharge (DBD) reactor. RSC Adv 12:10997–11007. https://doi.org/10.1039/D2RA01097F
23. Kleiman M, Ryu KA, Esser-Kahn AP (2016) Determination of factors influencing the wet etching of polydimethylsiloxane using tetra-*n*-butylammonium fluoride. Macromol Chem Phys 217:284–291. https://doi.org/10.1002/macp.201500225
24. Franclemont JT, Fan X, Li R, Singh RK, Holsen TM, Mededovic Thagard S (2018) Chemical reaction mechanisms accompanying pulsed electrical discharges in liquid methanol. Plasma Process Polym 15:1800019. https://doi.org/10.1002/ppap.201800019
25. Bothe E, Schuchmann MN, Schulte-Frohlinde D, Sonntag C (1978) HO_2 elimination from α-hydroxyalkylperoxyl radicals in aqueous solution. Photochem Photobiol 28:639–643. https://doi.org/10.1111/j.1751-1097.1978.tb06984.x
26. Peak MJ, Peak JG (1990) Hydroxyl radical quenching agents protect against DNA breakage caused by both 365-nm UVA and by gamma radiation. Photochem Photobiol 51:649–652. https://doi.org/10.1111/j.1751-1097.1990.tb01752.x
27. Detmer CA, Pamatong FV, Bocarsly JR (1996) Nonrandom double strand cleavage of DNA by a monofunctional metal complex: mechanistic studies. Inorg Chem 35:6292–6298. https://doi.org/10.1021/ic960089k
28. Aboubakr HA, Gangal U, Youssef MM, Goyal SM, Bruggeman PJ (2016) Inactivation of virus in solution by cold atmospheric pressure plasma: identification of chemical inactivation pathways. J Phys D:Appl Phys 49:204001. https://doi.org/10.1088/0022-3727/49/20/204001
29. Al-Nu'airat J, Dlugogorski BZ, Gao X, Zeinali N, Skut J, Westmoreland PR, Oluwoye I, Altarawneh M (2019) Reaction of phenol with singlet oxygen. Phys Chem Chem Phys 21:171–183. https://doi.org/10.1039/C8CP06273K
30. DeMaster EG, Quast BJ, Redfern B, Nagasawa HT (1995) Reaction of nitric oxide with the free sulfhydryl group of human serum albumin yields a sulfenic acid and nitrous oxide. Biochem 34:11494–11499. https://doi.org/10.1021/bi00034a030
31. Sankarapandi S, Zweier JL (1999) Evidence against the generation of free hydroxyl radicals from the interaction of copper, zinc-superoxide dismutase and hydrogen peroxide. J Biol Chem 274:34576–34583. https://doi.org/10.1074/jbc.274.49.34576

32. Jourd'heuil FL, Lowery AM, Melton EM, Mnaimneh S, Bryan NS, Fernandez BO, Park J-H, Ha C-E, Bhagavan NV, Feelisch M (2010) Redox-sensitivity and site-specificity of S-and N-denitrosation in proteins. PLoS ONE 5:e14400. https://doi.org/10.1371/journal.pone.0014400
33. Riordan E, Minogue N, Healy D, O'Driscol P, Sodeau JR (2005) Spectroscopic and optimization modeling study of nitrous acid in aqueous solution. J Phys Chem A 109:779–786. https://doi.org/10.1021/jp050690h
34. Brisset J-L, Pawlat J (2016) Chemical effects of air plasma species on aqueous solutes in direct and delayed exposure modes: discharge, post-discharge and plasma activated water. Plasma Chem Plasma Process 36:355–381. https://doi.org/10.1007/s11090-015-9661-9
35. Zhang Q, Ma R, Tian Y, Su B, Wang K, Yu S, Zhang J, Fang J (2016) Sterilization efficiency of a novel electrochemical disinfectant against *Staphylococcus aureus*. Environ Sci Technol 50:3184–3192. https://doi.org/10.1021/acs.est.5b05108
36. Pandey S, Jangra R, Ahlawat K, Mishra R, Mishra A, Jangra S, Prakash R (2023) Selective generation of nitrate and nitrite in plasma activated water and its physicochemical parameters analysis. Phys Lett A 474:128832. https://doi.org/10.1016/j.physleta.2023.128832
37. Kim M, Kim C, Lee H, Kim K (1996) Temperature dependence of dissociation constants for formic acid and 2, 6-dinitrophenol in aqueous solutions up to 175 C. J Chem Soc Faraday Trans 92:4951–4956. https://doi.org/10.1039/FT9969204951
38. Da Silva G, Kennedy EM, Dlugogorski BZ (2006) Ab initio procedure for aqueous-phase p K a calculation: the acidity of nitrous acid. J Phys Chem A 110:11371–11376. https://doi.org/10.1021/jp0605546
39. Betterton EA, Robinson JL (1997) Henry's law coefficient of hydrazoic acid. J Air Waste Manage Assoc 47:1216–1219. https://doi.org/10.1080/10473289.1997.10464060
40. White-Stevens RH, Stover LR (1982) Interference by ascorbic acid in test systems involving peroxidase. II. Redox-coupled indicator systems. Clin Chem 28:589–595. https://doi.org/10.1093/clinchem/28.3.589
41. Cleland WW (1964) Dithiothreitol, a new protective reagent for SH groups. Biochem 3:480–482. https://doi.org/10.1021/bi00896a020
42. Lackmann J-W, Bruno G, Jablonowski H, Kogelheide F, Offerhaus B, Held J, Schulz-von der Gathen V, Stapelmann K, von Woedtke T, Wende K (2019) Nitrosylation vs. oxidation–How to modulate cold physical plasmas for biological applications. PLoS ONE 14:e0216606. https://doi.org/10.1371/journal.pone.0216606
43. Broniowska KA, Diers AR, Hogg N (2013) S-Nitrosoglutathione. Biochim Biophys Acta - Gen Subj 1830:3173–3181. https://doi.org/10.1016/j.bbagen.2013.02.004
44. Keszler A, Zhang Y, Hogg N (2010) Reaction between nitric oxide, glutathione, and oxygen in the presence and absence of protein: How are S-nitrosothiols formed? Free Radic Biol Med 48:55–64. https://doi.org/10.1016/j.freeradbiomed.2009.10.033
45. Espey MG, Thomas DD, Miranda KM, Wink DA (2002) Focusing of nitric oxide mediated nitrosation and oxidative nitrosylation as a consequence of reaction with superoxide. Proc Natl Acad Sci U S A 99:11127–11132. https://doi.org/10.1073/pnas.182157099
46. Lukes P, Dolezalova E, Sisrova I, Clupek M (2014) Aqueous-phase chemistry and bactericidal effects from an air discharge plasma in contact with water: evidence for the formation of peroxynitrite through a pseudo-second-order post-discharge reaction of H_2O_2 and HNO_2. Plasma Sources Sci Technol 23:015019. https://doi.org/10.1088/0963-0252/23/1/015019
47. González-Mancebo S, García-Santos MP, Hernández-Benito J, Calle E, Casado J (1999) Nitrosation of phenolic compounds: Inhibition and enhancement. J Agric Food Chem 47:2235–2240. https://doi.org/10.1021/jf981243k
48. Von Gunten U (2003) Ozonation of drinking water: Part I. Oxidation kinetics and product formation. Water Res 37:1443–1467. https://doi.org/10.1016/S0043-1354(02)00457-8
49. Graves DB (2012) The emerging role of reactive oxygen and nitrogen species in redox biology and some implications for plasma applications to medicine and biology. J Phys D: Appl Phys 45:263001. https://doi.org/10.1088/0022-3727/45/26/263001

Publisher's Note Springer Nature remains neutral with regard to jurisdictional claims in published maps and institutional affiliations.